Journal of Solid State Chemistry 209 (2014) 63–68

Contents lists available at ScienceDirect

Journal of Solid State Chemistry

journal homepage: www.elsevier.com/locate/jssc

Synchrotron X-ray diffraction and Raman spectroscopy of Ln_3NbO_7 (Ln=La, Pr, Nd, Sm-Lu) ceramics obtained by molten-salt synthesis

K.P.F. Siqueira [a], J.C. Soares [a], E. Granado [b], E.M. Bittar [c], A.M. de Paula [d], R.L. Moreira [d], A. Dias [a,*]

[a] Departamento de Química, Universidade Federal de Ouro Preto, Campus Morro do Cruzeiro, ICEB II, Ouro Preto-MG 35400-000, Brazil
[b] Instituto de Física "Gleb Wataghin", UNICAMP, Campinas-SP 13083-970, Brazil
[c] Laboratório Nacional de Luz Síncrotron, C.P. 6192, 13083-970 Campinas-SP, Brazil
[d] Departamento de Física, ICEx, Universidade Federal de Minas Gerais, C.P. 702, Belo Horizonte-MG 30123-970, Brazil

ARTICLE INFO

Article history:
Received 11 July 2013
Received in revised form
7 October 2013
Accepted 9 October 2013
Available online 23 October 2013

Keywords:
Synchrotron X-ray diffraction
SHG
Rare-earth
Niobates
Raman spectroscopy

ABSTRACT

Ln_3NbO_7 (Ln=La, Pr, Nd, Sm, Eu, Gd, Tb, Dy, Ho, Er, Tm, Yb, and Lu) ceramics were obtained by molten-salt synthesis and their structures were systematically investigated by synchrotron X-ray diffraction (SXRD), second harmonic generation (SHG) and Raman spectroscopy. It was observed that ceramics with the largest ionic radii (La, Pr, Nd) crystallized into the *Pmcn* space group, while the ceramics with intermediate ionic radii (Sm-Gd) exhibited a different crystal structure belonging to the *Ccmm* space group. For this last group of ceramics, this result was corroborated by SHG and Raman scattering and ruled out any possibility for the non-centrosymmetric $C222_1$ space group, solving a recent controversy in the literature. Finally, according to SXRD, Tb-Lu containing samples exhibited an average defect fluorite structure ($Fm\bar{3}m$ space group). Nonetheless, broad scattering at forbidden Bragg reflections indicates the presence of short-range domains with lower symmetry. Vibrational spectroscopy showed the presence of six Raman-active modes, inconsistent with the average cubic fluorite structure, and in line with the existence of lower-symmetry nano-domains immersed in the average fluorite structure of these ceramics.

1. Introduction

In the last years, lanthanide-based ceramics of general formula Ln_3BO_7 (Ln is a trivalent lanthanide, while B can be Os, Re, Ru, Mo, Ir, Sb, Nb or Ta pentavalent cations) have attracted much attention because of their interesting dielectric, catalytic and magnetic properties [1–15]. The structure is derived from the *weberite* group ($A_2B_2\times_7$), an anion-deficient fluorite-related superstructure, as described by Nino et al. [4]. The crystal structure of Ln_3NbO_7 compounds is called *weberite*-type, since it is formed by an arrangement of BO_6 octahedra and LnO_8 cubes in layers. However, these *weberite*-like ceramics exhibit a different configuration with seven-fold coordination between the layers [4,7,9]. A variety of crystal structures has been proposed for the Ln_3BO_7 ceramics, as a direct consequence of the great number of chemical combinations that is possible between the lanthanide ions and the element B (Ta, Nb, Sb, Mo) [1–15]. Also, the processing conditions can contribute to produce different crystallographic structures; for example, several polymorphic modifications can be achieved through temperature changes [2,8,9,16].

Since the physical properties are strictly dependent on the crystalline phase, it is important to determine the correct crystal structure before designing any possible application for these ceramics. The pioneer work in this sense was published by Rossell [3], who proposed the *Cmcm* space group for the La_3NbO_7 ceramic. However, the *Pnma* space group was later employed by Kahn-Harari et al. [17] to describe this phase. In the literature, the *Cmcm* space group is more commonly found to describe the crystal structure of the Ln_3BO_7 family: Ln_3RuO_7 (Ln=La–Eu) [6,7,11,18,19], Ln_3ReO_7 (Ln=Pr, Nd, Sm–Tb) [20,21], Ln_3OsO_7 (Ln=Pr, Nd, Sm–Gd) [18–20], Ln_3TaO_7 (Ln=La–Nd) [22–24], Ln_3IrO_7 (Ln=Pr, Nd, Sm, Eu) [16,25,26], Pr_3NbO_7 [27] and Ln_3SbO_7 (Ln=La–Nd) ceramics [11,15,27]. For Ln_3TaO_7 (Ln=Y, Sm–Ho) [12] and Ln_3MoO_7 (Ln=La–Nd, Sm, Eu) ceramics [28,29], the $C222_1$ and $P2_12_12_1$ space groups were previously described, respectively. Besides, the $Fm\bar{3}m$ space group was found for Ln_3TaO_7 (Ln=Ho–Lu) [11,12] and Ln_3NbO_7 (Ln=Dy–Lu) ceramics [10,11]. The $C222_1$ space group was also employed to describe the structure of Ln_3NbO_7 with intermediate ionic radii Ln (Ln=Sm–Tb), while the *Pnma* space group was proposed for ceramics with larger ionic radii (Ln=La, Pr, Nd) [10]—in agreement with previous work by Kahn-Harari et al.

* Corresponding author. Tel.: +55 31 3559 1716.
E-mail addresses: anderson_dias@iceb.ufop.br, anderson_dias@ig.com.br (A. Dias).

0022-4596/$ - see front matter © 2013 Elsevier Inc. All rights reserved.
http://dx.doi.org/10.1016/j.jssc.2013.10.015

[17]. Other few studies have been carried out for Sb as pentavalent cation. In a pioneer work in the seventies, a series of Ln_3SbO_7 ceramics with Ln=Nd, Sm–Yb, and Y were reported by Nath as belonging to the pyrochlore ($Fd\bar{3}m$) structure [30]. Later on, Vente et al. proposed a fluorite related *Cmcm* group for Pr_3SbO_7 [27]. Then, Fennel et al. [31] proposed the $C222_1$ space group for Dy_3SbO_7 and Ho_3SbO_7. Recently, Hinatsu et al. [15] determined the *Cmcm* space group for Ln=La, Pr, Nd and $C222_1$ for Ln=Nd-Lu. However, Fu and Ijdo reported a critical, detailed study for all these structures and presented an alternative setting of the *Cmcm* space group, namely *Ccmm*, instead of $C222_1$, for Ln_3SbO_7 ceramics containing intermediate-sized lanthanides [32].

In this paper, we report the molten-salt synthesis of Ln_3NbO_7 ceramics (exception for Ce and Pm) in lower temperatures if compared with those commonly reported in the literature by using conventional solid-state reactions. Following, their crystal structures were deeply investigated by using SXRD, SHG and Raman spectroscopy. In a previous paper, Ln_3SbO_7 ceramics (Ln=La–Dy) were studied by these techniques [33] and their structures determined. In view of that, the same methodology was applied for our Ln_3NbO_7 ceramics. In the present literature, only one paper by Kovyazina et al. [34] reports the Raman spectra of La, Nd and Gd-containing ceramics. These authors emphasize the difficulties to obtain reliable data from Raman scattering for these materials because of the strong luminescence that could occur for some lanthanides. Thus, the present paper shows our efforts towards the determination of the crystal structures of Ln_3NbO_7 ceramics synthesized through molten-salt processing by using three powerful techniques, namely SXRD, Raman scattering and SHG.

2. Experimental

Ln_3NbO_7 materials were synthesized by molten-salt processing using Ln_2O_3 (Ln=La, Nd, Sm, Eu, Gd, Dy, Ho, Er, Tm, Yb, Lu, >99% Sigma-Aldrich), Tb_4O_7 (>99.9% Sigma-Aldrich), Pr_6O_{11} (>99.9% Sigma-Aldrich), and Nb_2O_5 (>99.9% Sigma-Aldrich) as starting materials. Stoichiometric amounts of the reactants were mixed and ground thoroughly. An excess amount of 10% weight of lanthanide oxide was added in all mixtures to avoid the formation of $LnNbO_4$ compounds. The mixed powders were calcined in a molten-salt flux of NaCl (Aldrich) at 1100 °C for times of 8 h (La, Pr, Nd, Sm, Eu, Gd, Ho, Er, and Lu), 16 h (Tb and Tm), and 24 h (Yb) with intermediate regrinding. Dy_3NbO_7 was the only one of its kind ceramic produced at 1300 °C, for 8 h. After synthesis, the resulting products were washed in hot distilled water and diluted nitric acid (0.1 M) to dissolve and remove the residual NaCl and lanthanide oxides, followed by drying at 80 °C.

High-resolution synchrotron X-ray diffraction (SXRD) measurements were taken in the X-ray diffraction and spectroscopy (XDS) beamline of the Brazilian Synchrotron Laboratory, LNLS, in flat plane geometry, at room temperature, with λ=0.65319 Å. The measurements were performed in the 2θ range of 4–50° (Ln=Nd, Sm, Gd, Dy, and Yb) or 4–90° (Ln=La and Tm), with a step size of 0.008°. Further details of the experimental setup are given in a previous work [33]. Rietveld refinements were performed using the suite GSAS+EXPGUI [35]. Unidentified impurity phases were detected for all investigated samples, with peak intensities less than ~5% of the main reflections, except for the Dy_3NbO_7 sample, where the impurity peaks are as intense as ~20% of the main reflections. Due to the high angular resolution of our experimental setup, the peak overlap between the impurity and main phase reflections are minimized, leading to reliable refined structural parameters for the main phases. For Ln=Gd–Yb, asymmetries or shoulders at the lower-angle side of the Bragg peaks were observed, which could be satisfactorily modeled by a second minority crystalline phase with the same space group of the main phase and slightly larger unit cell volume. Although the atomic occupations and positions could not be reliably refined for this minority phase, we suggest that it is a metastable state with slightly different stoichiometry and/or degree of Ln/Nb antisite disorder with respect to the main phase.

Second harmonic generation (SHG) measurements were also performed. SHG is only present in structures lacking inversion symmetry [36], hence this technique can be used to determine the presence of this symmetry operation. We have used a 140 fs Ti-Sapphire oscillator (Coherent Chameleon) with 80 MHz repetition tuned at 800 nm which is directed to a modified Olympus FV300 scanning laser microscope. The backscattered signal is then directed to a dichroic mirror and a thin band pass centered at second harmonic wavelength (400 nm) to completely remove the laser scattered light where the SHG signal is detected by a photomultiplier tube. We have used an alpha-quartz crystal with the laser incidence paralell to the *c*-axis as a reference for this measurement. The second harmonic emission from alpha-quartz is clearly detectable, although this material posses weak second order susceptibility (0.3 pm/V) compared to other materials [36].

Raman spectra of as-synthesized samples were collected in back-scattering configuration by using three different equipments. The first one was a triple-monochromator Jobin-Yvon T64000 spectrometer with an Olympus confocal microscope (80× objective), exciting lines of 488 and 514.5 nm of an Ar^+ laser (effective powers from 10 to 50 mW at the sample's surface), and a liquid-N_2-cooled charge coupled device (CCD) detector. The frequency resolution was better than 2 cm^{-1} and the accumulation times were typically 10 collections of 30 s. Also, a Dilor XY spectrometer (Olympus confocal microscope, 50× objective) equipped with the 568.2 nm line of a Kr^+ laser (1 mW at the sample's surface), 600 grooves/mm diffraction gratings and a liquid-N_2-cooled charge coupled device (CCD) detector. The spectral resolution was better than 2 cm^{-1} and the accumulation times were typically 10 collections of 40 s. Finally, an Horiba/Jobin-Yvon LABRAM-HR spectrometer was used with the 632.8 nm line of a helium–neon laser (effective power of 6 mW at the sample's surface) as excitation source, diffraction gratings of 600 and 1800 grooves/mm, Peltier-cooled CCD detector, confocal Olympus microscope (100× objective), and experimental resolution of typically 1 cm^{-1} for 10 accumulations of 30 s. All experimental spectra were corrected by the Bose–Einstein thermal factor [37].

3. Results and discussion

SXRD experiments were performed for Ln_3NbO_7 with Ln=La, Nd, Sm, Gd, Dy, Tm, and Yb. Fig. 1(a–c) show SXRD profiles for Ln=La, Gd, and Tm, respectively, which reveal all the representative crystalline phases observed in this series at room temperature. The refined structural data for Ln=Nd, Sm, Dy, and Yb are given as Supplementary materials (Tables 1–4). For the largest lanthanides, Ln=La and Nd, the structure was successfully refined under the orthorhombic *Pmcn* space group, which is an alternative setting of the *Pnma* space group, in line with previous reports [10,17,38]. This structure is less symmetrical than that of La_3SbO_7 with *Cmcm* space group, as revealed by the observation of a number of weak reflections forbidden for a *C* lattice. The refined structural parameters for Ln=La are given in Table 1. A noteworthy difference between the structures of Ln_3NbO_7 and Ln_3SbO_7 for Ln=La–Nd [33] is that the Sb position is centered with respect to the oxygen octahedra in the latter, while the Nb is off-centered in the former. This can be attributed to the strong tendency of Nb^{5+} towards

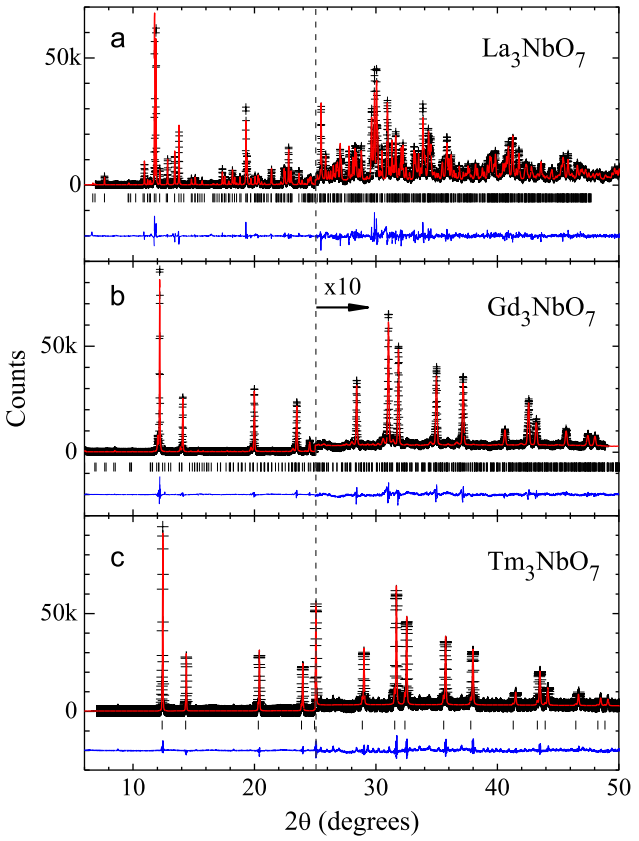

Fig. 1. SXRD patterns of Ln_3NbO_7 for (a) Ln=La, (b) Ln=Gd, and (c) Ln=Tm with λ=0.65319 Å. The cross symbols and solid lines represent observed and calculated patterns, respectively. The difference curves are shown at the bottom of each figure. Vertical bars indicate the expected Bragg peak positions according to the crystal structure models described in the text and refined lattice parameters given in Tables 1–3.

Table 1
Refined structural parameters for La_3NbO_7.

Atom	Site	x	y	z	B (Å^2)
La(1)	4*c*	0.25	0.7714(2)	0.0054(4)	0.51(2)
La(2)	8*d*	0.47578(9)	0.44948(12)	0.2501(3)	0.51(2)
Nb	4*c*	0.25	0.2554(5)	0.9949(12)	1.04(6)
O(1)	8*d*	0.8738(12)	0.945(2)	0.962(2)	0.51(11)
O(1′)	8*d*	0.3782(12)	0.417(2)	0.963(2)	0.51(11)
O(2)	8*d*	0.3806(9)	0.7258(12)	0.250(4)	0.51(11)
O(3)	4*c*	0.25	0.306(2)	0.230(3)	0.51(11)

Note: Space group *Pmcn*, a=11.1663(3) Å, b=7.6342(2) Å, c=7.7555(2) Å, V=661.12 (4) Å^3, R_{wp}=16.2%, R_p=10.7%.

asymmetric bonding, leading in many cases to ferroelectricity in Nb-based compounds.

For medium-sized lanthanides, Ln=Sm and Gd, the crystal structure was successfully refined under the *Ccmm* space group, similar to Ln_3SbO_7 (Ln=Sm-Gd) [33]. The less symmetrical space group $C222_1$, employed in Ref. [10] for the same compounds, was also tested. Nonetheless, the goodness of fit χ^2 and fitting residuals R_{wp} are nearly identical for refinements under both space groups. A direct evidence against the space group $C222_1$ is the absence, within our sensitivity (~0.05% of the most intense Bragg peak), of the extra reflection (0 2 1) at 2θ=11.07°, predicted for this space group and forbidden for *Ccmm*. This conclusion is further supported by the absence of SHG signal (which indicates the existence of inversion symmetry center in the crystal structure) and by our Raman scattering (see discussion below). Cai et al. [5] observed a non-centrosymmetric structure for the sample containing Gd

Table 2
Refined structural parameters for Gd_3NbO_7.

Atom	Site	x	y	z	B (Å^2)
Gd(1)	4*b*	0	0.5	0	2.35(7)
Gd(2)	8*g*	0.2464(3)	0.2446(4)	0.25	2.35(7)
Nb	4*a*	0	0	0	0.7(2)
O(1)	16*h*	0.118(4)	0.210(2)	0.977(2)	3.3(3)
O(2)	4*c*	0.101(4)	0.5	0.25	3.3(3)
O(2′)	4*c*	0.907(4)	0.5	0.25	3.3(3)
O(3)	4*c*	0.077(4)	0	0.25	3.3(3)

Note: Space group *Ccmm*, a=10.6375(4) Å, b=7.5229(3) Å, c=7.5417(3) Å, V=603.52(4) Å^3, R_{wp}=15.0%, R_p=10.6%.

Table 3
Refined structural parameters for Tm_3NbO_7.

Atom	Site	occupancy	x	y	z	B (Å^2)
Tm	4*a*	0.75	0	0	0	2.35(2)
Nb	4*a*	0.25	0	0	0	2.35(2)
O	8*c*	0.875	0.25	0.25	0.25	5.0(2)

Note: Average space group $Fm\bar{3}m$, a=5.2131(2) Å, V=141.67(2) Å^3, R_{wp}=15.5%, R_p=10.9%.

(*Cm2m*, #38) at room temperature, which changed for a *Cmcm* space group above 340 K. However, the low-symmetry structure with *Cm2m* space group reported in Ref. [5] is not compatible with our room temperature SXRD data for Ln=Gd. In fact, both SXRD and SHG data indicate that our sample is centrosymmetric at room temperature, probably due to the significant differences between the employed processing routes. Cai et al. [5] produced their samples by sintering at 1600 °C from solid-state reacted powders, while our samples were obtained directly at 1100 °C by molten-salt synthesis. The refined structural parameters for our Gd_3NbO_7 ceramics are given in Table 2. Contrary to the Ln_3NbO_7 structure with large Ln, described under *Pmcn* space group with off-centered NbO_6 octahedra rotated around the [1 0 0] axis, the structure for medium-sized Ln shows centered NbO_6 octahedra rotated around the [0 1 0] axis (see also Fu and Ijdo, Ref. [32]).

For small-sized lanthanides (Ln=Dy, Tm and Yb), a symmetrization of the average structure is observed, and a defect CaF_2 structure with cubic space group $Fm\bar{3}m$ was successfully employed in the refinements, in line with previous reports [1,10]. A pyrochlore structure ($Fd\bar{3}m$ space group) with doubled lattice parameter with respect to the $Fm\bar{3}m$ structure was also attempted to describe the diffraction profiles of such materials. Nonetheless, the extra Bragg peaks expected for the pyrochlore structure were not observed within our sensitivity, indicating that the space group $Fm\bar{3}m$ describes the symmetry of the average structure of these materials. The refined structural parameters for Ln=Tm are given in Table 3.

Fig. 2 shows the X-ray scattering signal at the vicinity of the weak 1 1 0 reflection (*Ccmm* setting) for Ln ranging from Sm to Yb. For Ln=Sm, a sharp 110 reflection at Q=1.02 Å^{-1} and other minor peaks consistent with the *Ccmm* space group are observed, while for Ln=Gd a sharp reflection appear to coexist with a broad scattering at this position. For Ln=Dy, Tm and Yb, this reflection is forbidden for the cubic $Fm\bar{3}m$ structure, although a broad scattering persists at the vicinity of this position. This indicates short-range structural domains that may be related to ordering of Ln/Nb cations and/or oxygen vacancies. This possibility is supported by our Raman scattering data described below and also by recent selected area electron diffraction and high-resolution transmission electron microscopy (HRTEM) in Ln_3NbO_7 (Ln=Y, Er, Yb, and Lu) [39]. From the full width at half maximum of the

Table 4
Factor-group analysis for all crystal structures previously reported by the literature for the Ln_3NbO_7 materials. Only the Raman-active irreducible representations at the Brillouin-zone center (Γ) were considered.

Ion	Wyckoff sites	Symmetry	Irreducible representations
Cubic fluorite-type ($Fm\bar{3}m$, #225)			
Ln^{+3}	4*a*	O_h	No Raman-active
Nb^{+5}	4*a*	O_h	No Raman-active
O^{-2}	8*c*	T_d	F_{2g}
$\Gamma_{RAMAN}=F_{2g}$			
Cubic pyrochlore ($Fd\bar{3}m$, #227)			
Ln^{+3}	16*c*	O_h	No Raman-active
Nb^{+5}	16*d*	O_h	No Raman-active
$O^{-2}(1)$	48*f*	O_h	$A_{1g}+E_g+3F_{2g}$
$O^{-2}(2)$	8*a*	O_h	F_{2g}
$\Gamma_{RAMAN}=A_{1g}+E_g+4F_{2g}$			
Orthorhombic (*Ccmm*, #63)			
$Ln^{+3}(1)$	4*a*	C_{2h}^{x}	No Raman-active
$Ln^{+3}(2)$	8*g*	C_s^{xy}	$2A_g+2B_{1g}+B_{2g}+B_{3g}$
Nb^{+5}	4*b*	C_{2h}^{x}	No Raman-active
$O^{-2}(1)$	4*c*	C_{2h}^{y}	$A_g+B_{1g}+B_{3g}$
$O^{-2}(2)$	16*h*	C_1	$3A_g+3B_{1g}+3B_{2g}+3B_{3g}$
$O^{-2}(3)$	8*g*	C_s^{xy}	$2A_g+2B_{1g}+B_{2g}+B_{3g}$
$\Gamma_{RAMAN}=8A_g+8B_{1g}+5B_{2g}+6B_{3g}$			
Orthorhombic (*Pmcn*, #62)			
$Ln^{+3}(1)$	4*c*	C_s^{xz}	$2A_g+B_{1g}+2B_{2g}+B_{3g}$
$Ln^{+3}(2)$	8*d*	C_1	$3A_g+3B_{1g}+3B_{2g}+3B_{3g}$
Nb^{+5}	4*c*	C_s^{xz}	$2A_g+B_{1g}+2B_{2g}+B_{3g}$
$O^{-2}(1)$	8*d*	C_1	$3A_g+3B_{1g}+3B_{2g}+3B_{3g}$
$O^{-2}(2)$	8*d*	C_1	$3A_g+3B_{1g}+3B_{2g}+3B_{3g}$
$O^{-2}(3)$	8*d*	C_1	$3A_g+3B_{1g}+3B_{2g}+3B_{3g}$
$O^{-2}(4)$	4*c*	C_s^{xz}	$2A_g+B_{1g}+2B_{2g}+B_{3g}$
$\Gamma_{RAMAN}=18A_g+15B_{1g}+18B_{2g}+15B_{3g}$			
Orthorhombic ($C222_1$, #20)			
$Ln^{+3}(1)$	4*b*	C_2^{y}	$A+2B_1+B_2+2B_3$
$Ln^{+3}(2)$	8*c*	C_1	$3A+3B_1+3B_2+3B_3$
Nb^{+5}	4*b*	C_2^{y}	$A+2B_1+B_2+2B_3$
$O^{-2}(1)$	8*c*	C_1	$3A+3B_1+3B_2+3B_3$
$O^{-2}(2)$	8*c*	C_1	$3A+3B_1+3B_2+3B_3$
$O^{-2}(3)$	4*a*	C_2^{x}	$A+2B_1+2B_2+B_3$
$O^{-2}(4)$	4*a*	C_2^{x}	$A+2B_1+2B_2+B_3$
$O^{-2}(5)$	4*a*	C_2^{x}	$A+2B_1+2B_2+B_3$
$\Gamma_{RAMAN}=14A+19B_1+17B_2+16B_3$			

broad peaks ($\Delta q\sim 0.1$–0.15 Å^{-1}), the average size of the ordered domains are estimated as $2\pi/\Delta q\sim 40$–60 Å, which seems to be consistent with reported HRTEM data on the same system [39].

Raman scattering besides theoretical factor-group analysis are currently employed by our research group to investigate the behavior of the phonon modes in electroceramics. In this work, Raman scattering was used for all the Ln_3NbO_7 ceramics to confirm the results from SXRD and SHG techniques, aiming to show the relationship between crystal structure and vibrational modes, which allowed us to contribute to the debate on the crystalline structure of this class of ceramics. For compounds belonging to the cubic fluorite-type structure ($Fm\bar{3}m$, #225, O_h^5), *Ln* and Nb atoms are in the 4*a* sites (O_h symmetry), and O ions in the 8*c* sites (T_d symmetry). Using the site group method of Rousseau et al. [40], the distribution of the phonon modes at the Brillouin zone center can be obtained (Table 4). The results show that only one Raman-active mode is expected (F_{2g}). Cubic pyrochlore structures ($Fd\bar{3}m$, #227, O_h^7) presents *Ln* ions located in the 16*c* sites (O_h symmetry), Nb Atoms located in the 16*d* sites (O_h symmetry), and two kinds of oxygen atoms located in the 8*a* (O_h symmetry) and 48*f* sites (O_h symmetry). The site group method of Rousseau et al. [40] leads to the following distribution of the phonon modes at the Brillouin zone center: $A_{1g}+E_g+4F_{2g}$. Thus, six Raman-active modes are expected for cubic $Fd\bar{3}m$ structures. For the orthorhombic *Ccmm* space-group (#63, D_{2h}^{17}), two kinds of lanthanide atoms and three different oxygen atoms can be found: *Ln*(1) is located in the 4*a* sites (C_{2h}^{x} symmetry), *Ln*(2) is located in the 8*g* sites (C_s^{xy} symmetry), Nb atoms are located in the 4*b* sites (C_{2h}^{x} symmetry), O(1)-O(3) are respectively in the 4*c* (C_{2h}^{y} symmetry), 16*h* (C_1 symmetry), and 8*g* (C_s^{xy} symmetry) sites. The site group method of Rousseau et al. [40] leads to the following distribution of the phonon modes at the Brillouin zone center: $8A_g+8B_{1g}+5B_{2g}+6B_{3g}$. Thus, 27 Raman-active modes are expected in that *Ccmm* space-group (Table 4).

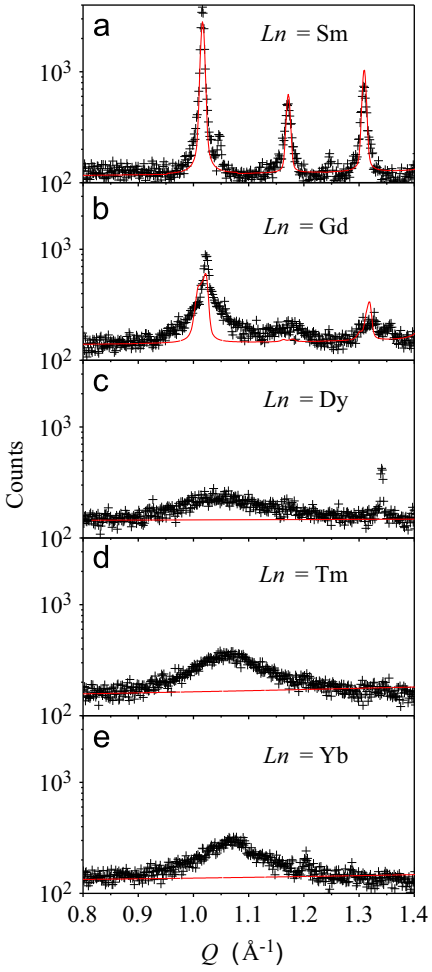

Fig. 2. X-ray scattering signal at the vicinity of the 1 1 0 reflection (*Ccmm* setting) for Ln_3NbO_7 with *Ln* ranging from Sm to Yb.

The other two possibilities for the crystal structures studied in the present work are presented below. The orthorhombic *Pmcn* space-group (#62, D_{2h}^{16}), an alternative setting of the *Pnma* space group, contains two kinds of lanthanide atoms and four different oxygen atoms: *Ln*(1) is located in the 4*c* sites (C_s^{xz} symmetry), *Ln*(2) is located in the 8*d* sites (C_1 symmetry), Nb atoms are located in the 4*c* sites, O(1)–O(3) are in the 8*c* sites, and the O(4) is located in the 4*c* sites. The method of Rousseau et al. [40] was then applied and the following distribution of the phonon modes at the Brillouin zone center can be obtained: $18A_g+15B_{1g}+18B_{2g}+15B_{3g}$. For this structure, 66 Raman-active modes are expected. Finally, the orthorhombic $C222_1$ (#20) space-group shows two kinds of lanthanide ions and five different oxygen ions in the following crystallographic sites: *Ln*(1) in the 4*a* sites (C_2^{x} symmetry), *Ln*(2) in the 8*c* sites (C_1 symmetry), Nb ions in the 4*b* sites (C_2^{y} symmetry), O(1)–O(2) in the 8*c* sites, and O(3)–O(5) in the 4*b* sites. In this case, the site group method of Rousseau et al. [40] leads to the following

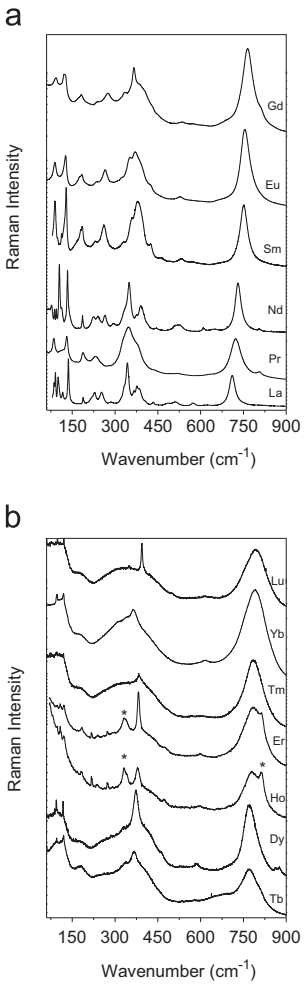

Fig. 3. Room-temperature Raman spectra for all Ln_3NbO_7 ceramics: (a) La–Gd, and (b) Tb–Lu. Extra bands are due to electronic artifacts and are indicated by asterisks.

distribution of the phonon modes at the Brillouin zone center: $14A+19B_1+17B_2+16B_3$. Excluding the acoustic and silent modes, 63 bands are also expected in the Raman spectra for this structure.

Raman spectra were experimentally obtained at room-temperature by using different excitation lines for all samples, in order to avoid strong luminescence and electronic transitions. The final spectra represent the best results obtained using the blue line (488 nm), for Eu, Gd, and Yb; yellow line (568.2 nm), for Ho and Er; and the red line (632.8 nm), for La, Pr, Nd, Sm, Tb, Dy, Tm, and Lu. The results are displayed in Fig. 3 (two boards) for decreasing ionic radius (La–Lu). It is well known that it is very difficult to analyze quantitatively the experimental results from Raman scattering in crystal structures with high number of predicted bands. Kovyazina et al. [34] studied La_3NbO_7, Nd_3NbO_7, Gd_3NbO_7 and Y_3NbO_7 materials and emphasized the difficulties to obtain reliable spectra.

As it can be noted in Fig. 3, the samples exhibited very complex spectra, which could be divided in three distinct groups, as follows. The first group of spectra encompasses La, Pr, and Nd-containing ceramics with similar set of vibrational bands, assumed as belonging to the *Pmcn* structure, as verified by the SXRD analysis. Particularly, the main features include the NbO_6 breathing mode at 710–730 cm^{-1} and a complex group of modes between 85 cm^{-1} and 400 cm^{-1}. The spectrum for the Pr_3NbO_7 ceramic presents rather broader bands besides strong down-shifted low-frequency modes (below 150 cm^{-1}), which could be probably linked to the proximity of a structural phase transition, as

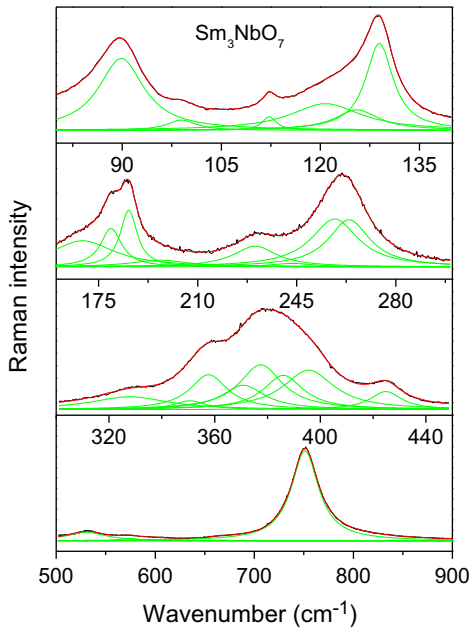

Fig. 4. Raman spectra for Sm_3NbO_7 ceramics belonging to the *Ccmm* space-group. Experimental data are in closed squares, whereas the fitting curves are represented by red lines. Green lines represent the phonon modes adjusted by Lorentzian curves. The Raman spectra were divided in four regions for better visualization.

previously observed in $CeNbO_4$ materials [41]. For this set of ceramics, it was expected 66 Raman-active modes (Table 4). However, no more than 27 bands could be observed (see Table 5 in Supplementary materials). It turns out this is the expected number of modes for the structure with *Cmcm* space group reported in the early works on similar Ln_3SbO_7 [33]. This result highlights the similarity between the structures with *Cmcm* and *Pmcn* space groups, suggesting that the extra modes presumably activated by the off-centering of NbO_6 octahedra in the *Pmcn* structure show very weak Raman activity and could not be observed within our sensitivity.

The second group of Raman spectra is formed by the samples Sm_3NbO_7, Eu_3NbO_7, and Gd_3NbO_7, which presented a significant up-shifting of the NbO_6 breathing mode if compared with the same mode for the previous group of ceramics. Also, down-shift of the low-frequency modes below 150 cm^{-1} and strong changes in the modes ranging from 150 to 450 cm^{-1} can be easily observed. In this respect, the mode at 380 cm^{-1} appears as a signature or a fingerprint of the orthorhombic *Ccmm* structure, as verified for Ln_3SbO_7 ceramics in a previous paper [33]. The adjustment of the experimental data through fitting procedures by Lorentzian curves was conducted for all samples and the results for the Sm_3NbO_7 ceramics are presented in Fig. 4. As a general trend, the wavenumbers of the bands down-shifted for decreasing ionic radii, as expected [42]. Raman modes obtained after fitting are presented for Sm, Eu, and Gd ceramics as Supplementary materials (Table 5). It is worthy noticing that 27 bands were depicted for these spectra, in perfect agreement with group theoretical predictions for the *Ccmm* space group.

Finally, the last group of ceramics includes Tb, Dy, Ho, Er, Tm, Yb, and Lu. For these materials, it is first observed an additional up-shift in the NbO_6 breathing mode. Also, the general Raman pattern has modified completely, with a large dominating band besides few very intense, discernible modes. Particularly, there are two low-frequency modes at 92–95 cm^{-1} and 1180,123 cm^{-1}, the band around 175–180 cm^{-1}, the mode around 370–390 cm^{-1}, and the bands around 765–794 cm^{-1}. Some extra Raman bands (marked by asterisks in Fig. 3b) were observed in samples with

Ho and Er, for which it is very difficult to obtain spectra free of electronic artifacts. According to SXRD analysis, for an average $Fm\bar{3}m$ structure, one would expect only one Raman-active band for this set of ceramics. However, our results showed that six modes are present, which are compatible with a cubic pyrochlore ($Fd\bar{3}m$) structure (see also Table 5 in Supplementary materials). This is consistent with our SXRD data shown in Fig. 2, which indicates the presence of lower-symmetry structural domains immersed in the $Fm\bar{3}m$ matrix for this last group of ceramics. In fact, once Raman spectroscopy is sensitive to the atomic structure in the nanometric range, is expected to capture the Raman-active modes of low-symmetry structural domains, explaining the observation of a higher number of observed modes with respect to that expected for the high-symmetry $Fm\bar{3}m$ structure. Corroborating our findings, López-Conesa et al. [39] also observed low-symmetry nano-domains in Ln_3NbO_7 (Ln=Y, Er, Yb, and Lu) by high-resolution transmition electron microscopy.

4. Conclusions

Ln_3NbO_7 (Ln=La, Pr, Nd, Sm, Eu, Gd, Tb, Dy, Ho, Er, Tm, Yb, and Lu) ceramics were synthesized by the molten-salt technique at lower temperatures if compared with those currently employed in conventional solid-state processing. The crystal structures of these materials were investigated by SXRD, SHG and Raman scattering. Orthorhombic and cubic structures were observed depending upon of the ionic radii of the lanthanide elements. It was observed that La-Nd based materials belong to *Pmcn* space group, while Sm-Gd samples belong to the *Ccmm* structure. For this group of ceramics, the results are in perfect agreement with the group-theory calculations and corroborate the results from SXRD and SHG analyses. According to SXRD, ceramics containing Tb-Lu exhibit an average defect fluorite $Fm\bar{3}m$ cubic structure with the presence of nano-domais with lower symmetry. The existence of such low-symmetry domains is also indicated by the observation of six Raman-active bands for these ceramics, in contrast to a single mode expected for the average $Fm\bar{3}m$ structure.

Acknowledgments

The authors thank the financial support from CNPq, FINEP and FAPEMIG. Special thanks to Dr. A. Righi, Dr. C. Fantini Leite, and Dr. M. A. Pimenta (UFMG) for their hospitality during Raman experiments with the Dilor XY and T64000 equipments. LNLS is acknowledged for concession of beamtime.

Appendix A. Supplementary material

Supplementary data associated with this article can be found in the online version at http://dx.doi.org/10.1016/j.jssc.2013.10.015.

References

[1] H.P. Rooksby, E.A.D. White, J. Am. Ceram. Soc. 47 (1964) 94.
[2] J.G. Allpress, H.J. Rossell, J. Solid State Chem. 27 (1979) 105.
[3] H.J. Rossell, J. Solid State Chem. 27 (1979) 115.
[4] L. Cai, J.C. Nino, Acta Crystallogr., Sect. B: Struct. Sci. 65 (2009) 269.
[5] L. Cai, S. Denev, V. Gopalan, J. Nino, J. Am. Ceram. Soc. 93 (2010) 875.
[6] P. Khalifah, Q. Huang, J.W. Lynn, R.W. Erwin, R.J. Cava, Mater. Res. Bull. 35 (2000) 1.
[7] D. Harada, Y. Hinatsu, J. Solid State Chem. 158 (2001) 245.
[8] D. Harada, Y. Hinatsu, J. Solid State Chem. 164 (2002) 163.
[9] N. Ishizawa, K. Tateishi, S. Kondo, T. Suwa, Inorg. Chem. 47 (2008) 558.
[10] Y. Doi, Y. Harada, Y. Hinatsu, J. Solid State Chem. 182 (2009) 709.
[11] M. Wakeshima, Y. Hinatsu, J. Solid State Chem. 183 (2010) 2681.
[12] M. Wakeshima, H. Nishimine, Y. Hinatsu, J. Phys. Condens. Matter 16 (2004) 4103.
[13] R. Abe, M. Higashi, Z. Zou, K. Sayama, Y. Abe, H. Arakawa, J. Phys. Chem. B 108 (2004) 811.
[14] L. Cai, J.C. Nino, J. Eur. Ceram. Soc. 27 (2007) 3971.
[15] Y. Hinatsu, H. Ebisawa, Y. Doi, J. Solid State Chem. 182 (2009) 1694.
[16] Y. Hinatsu, Y. Doi, H. Nishimine, M. Wakeshima, M. Sato, J. Alloys Compd. 488 (2009) 541.
[17] A. Kahn-Harari, L. Mazerolles, D. Michel, F. Robert, J. Solid State Chem. 116 (1995) 103.
[18] F. Wiss, N.P. Raju, A.S. Wills, J.E. Greedan, Int. J. Inorg. Mater. 2 (2000) 53–59.
[19] D. Harada, Y. Hinatsu, Y. Ishii, J. Phys. Condens. Matter 13 (2001) 10825–10836.
[20] R. Lam, T. Langet, J.E. Greedan, J. Solid State Chem. 171 (2002) 317–323.
[21] Y. Hinatsu, M. Wakeshima, N. Kawabuchi, N. Taira, J. Alloys Compd. 374 (2004) 79–83.
[22] J.R. Plaisier, R.J. Drost, D.J.W. IJdo, J. Solid State Chem. 169 (2002) 189–198.
[23] W.R. Gemmill, M.D. Smith, Y.A. Mozharivsky, G.J. Miller, H.-C. zur Loye, Inorg. Chem. 44 (2005) 7047–7055.
[24] R. Lam, F. Wiss, J.E. Greedan, J. Solid State Chem. 167 (2002) 182–187.
[25] J.F. Vente, D.J.W. IJdo, Mater. Res. Bull. 26 (1991) 1255–1262.
[26] H. Nishimine, M. Wakeshima, Y. Hinatsu, J. Solid State Chem. 177 (2004) 739–744.
[27] J.F. Vente, R.B. Helmholdt, D.J.W. IJdo, J. Solid State Chem. 108 (1994) 18–23.
[28] J.E. Greedan, N.P. Raju, A. Wegner, P. Gougeon, J. Padiou, J. Solid State Chem. 129 (1997) 320–327.
[29] H. Nishimine, M. Wakeshima, Y. Hinatsu, J. Solid State Chem. 178 (2005) 1221–1229.
[30] D.K. Nath, Inorg. Chem. 9 (1970) 2714–2718.
[31] T. Fennell, S.T. Bramwell, M.A. Green, Can. J. Phys. 79 (2001) 1415–1419.
[32] W.T. Fu, D.J.W. IJdo, J. Solid State Chem. 182 (2009) 2451–2455.
[33] K.P.F. Siqueira, R.M. Borges, E. Granado, L.M. Malard, A.M. de Paula, E.M. Bittar, R.L. Moreira, A. Dias, J. Solid State Chem. 203 (2013) 326–332.
[34] S.A. Kovyazina, L.A. Perelyaeva, I.A. Leonidov, Y.A. Bakhteeva, J. Struct. Chem. 44 (2003) 975.
[35] A.C. Larson, R.B. Von Dreele, Los Alamos National Laboratory Report LAUR 86–748 (2000);
B.H. Toby, J. Appl. Crystallogr. 34 (2001) 210–213.
[36] R.W. Boyd, Non Linear Optics, third ed., Academic Press, Burlington, MA, 2008.
[37] W. Hayes, R. Loudon, Scattering of Light by Crystals, Wiley, New York, 1978.
[38] L. Cai, J.C. Nino, J. Solid State Chem. 184 (2011) 2263.
[39] L. López-Conesa, J.M. Rebled, M.H. Chambrier, K. Boulahya, J.M. González-Calbet, M.D. Braida, G. Dezanneau, S. Estradé, F. Peiró, Fuel Cells 13 (2013) 29.
[40] D.L. Rousseau, R.P. Bauman, S.P.S. Porto, J. Raman Spectrosc. 10 (1981) 253.
[41] J. Yang, Y. Su, H. Li, X. Liu, Z. Chen, J. Alloys Compd. 509 (2011) 8008.
[42] K.P.F. Siqueira, R.L. Moreira, A. Dias, Chem. Mater. 22 (2010) 2668.